Interdomain Mobility in Di-Ubiquitin Revealed by NMR

Yaroslav Ryabov and David Fushman[*]
Department of Chemistry and Biochemistry, Center for Biomolecular Structure and Organization, University of Maryland, College Park, Maryland

ABSTRACT   Domain orientation and dynamics can play an essential role in the function of multidomain proteins. Lys48-linked polyubiquitin chains, the principal signal for proteasomal protein degradation, adopt a closed conformation at physiological conditions, in which the functionally important residues Leu8, Ile44, and Val70 are sequestered at the interdomain interface. This interface must open in order for these groups to become available for interactions with various chain-recognition factors. Knowledge of the mechanism of domain motion leading to the opening of the interdomain interface in polyubiquitin is, therefore, essential for the understanding of the processes controlling molecular recognition events in polyubiquitin signaling. Here we use NMR to characterize the interdomain dynamics that open the interface in a di-ubiquitin chain. This process occurs via domain reorientations on a 10-ns time scale and with the amplitudes that are sufficient for making functionally important hydrophobic residues in polyubiquitin available for direct interactions with various ubiquitin-binding factors. The analysis revealed the structures of the interconverting conformational states of di-ubiquitin and the rates and amplitudes of this process at near-physiological and acidic pH. The proposed mechanism of domain reorientation is quite general and could serve as a paradigm of interdomain mobility in other multidomain systems. Proteins 2006;63:787–796. © 2006 Wiley-Liss, Inc.

Key words: polyubiquitin; domain motion; interdomain orientation; spin relaxation; anisotropic diffusion

INTRODUCTION

Interdomain orientation and flexibility often play a key role in molecular recognition events and functional regulation in a variety of processes involving multidomain proteins, (e.g., Refs. 1–3). However, despite recent advances in structure characterization of multidomain systems and changes in interdomain orientation induced by ligand binding in solution (e.g., Refs. 4–8), very little is known about the actual mechanisms of interdomain dynamics in proteins. In a specific example considered here, Lys48-linked polyubiquitin (polyUb) chains, the principal signal for proteasomal protein degradation,[9,10] adopt a closed conformation under physiological conditions, in which the interdomain interface is formed by the hydrophobic surfaces on ubiquitin (Ub) domains comprising residues Leu8,

Ile44, and Val70.[11–13] In contrast, no definitive interface was observed at pH4.5[11] suggesting that the conformation of the chain is predominantly open under these conditions. It has been proposed[11] based on pH titration data that the Ub/Ub interface is not rigidly locked even at physiological pH and is in dynamic equilibrium between closed and open conformations. The sequestration of the functionally important hydrophobic residues at the interface, therefore, could regulate ligand binding to polyUb, wherein the Ub/Ub interface must open in order for these sites to become available for interactions with various chain-recognition factors. In support of this model, direct ligand binding to the interface residues was observed in di-ubiquitin (Ub$_2$) at pH6.8,[11,14,15] whereas restricting the domain motion by site-directed cross-linking rendered Ub$_2$ binding-incompetent (Fushman, forthcoming). Knowledge of the mechanism of domain motion in polyUb is, therefore, essential for the understanding of the factors regulating ligand binding to these chains and could shed light on the processes controlling molecular recognition events in polyUb signaling.

NMR relaxation data indicate that, although to a good approximation the two Ub domains in Lys48-linked Ub$_2$ tumble together as a single molecular entity rather than as completely independent "beads on a flexible string,"[8,11] this molecule still possesses some interdomain motion. This conclusion follows from the observed discrepancies in the rotational diffusion tensors of Ub$_2$ "reported" by the individual Ub domains (Table I). Specifically, there is a difference, most pronounced at pH 6.8, in the overall tumbling rates experienced by the two domains (note that the overall tumbling reported by both domains in Ub$_2$ is approximately twofold slower than in monomeric Ub). Moreover, the rotational diffusion tensor measured in the distal Ub is almost axially symmetric, whereas that for the proximal Ub shows lesser anisotropy but significantly greater rhombicity, resembling that for an oblate rather than a prolate object. This is in contrast with the overall shape of Ub$_2$ and with hydrodynamic calculations for a

TABLE I. Experimental and Predicted Characteristics of the Overall Rotational Diffusion Tensor for Lys48-Linked Ub$_2$, Derived Neglecting the Interdomain Motion

	D_x^a	D_y^a	D_z^a	τ_c^b	Anisotropy^c	Rhombicity^d
NMR, pH6.8:						
Proximal domain^e	1.68	2.06	2.30	8.28	1.23	1.33
Distal domain^e	1.73	1.86	2.69	7.96	1.50	0.22
NMR, pH4.5:						
Proximal domain^e	1.78	2.00	2.15	8.44	1.14	1.27
Distal domain^e	1.69	1.77	2.50	8.39	1.45	0.16
Theory^f						
1AAR^f	1.57	1.59	2.44	8.94	1.54	0.04
2BGF^f	1.46	1.49	2.39	9.37	1.62	0.06
	(0.04)	(0.05)	(0.07)	(0.27)	(0.02)	(0.01)

^{a}Principal values, D_x, D_y, D_z, of the overall rotational diffusion tensor, in 10^7 s^{-1} (ordered as $D_x \leq D_y \leq D_z$).
^{b}The overall rotational correlation time of the molecule, $\tau_c = [2 \cdot \mathrm{tr}(\underline{\underline{D}})]^{-1}$, in 10^{-9} s.
^{c}Anisotropy of the diffusion tensor, defined as $2D_z/(D_x + D_y)$.
^{d}Rhombicity of the diffusion tensor, defined as $3/2(D_y - D_x)/[D_z - 1/2(D_x + D_y)]$.
^{e}"Proximal" and "distal" refer to Ub's position in the chain with respect to the free C-terminus.
^{f}Theoretical predictions for the diffusion tensor of Ub$_2$ from hydrodynamic calculations using HYDRONMR[34] program with the shell model atomic element radius of 3.0 A. The Ub$_2$ atom coordinates were from PDB entries 1AAR[12] and 2BGF[13] as indicated. In the latter set, the results are averaged over an ensemble of 10 NMR structures (pH 6.8), the numbers in parentheses indicate standard deviations within the ensemble. The unstructured in solution four C-terminal residues of the proximal domain were clipped off in both calculations.

rigid Ub$_2$ molecule (Table I) predicting an axially symmetric rotational diffusion tensor with higher anisotropy than that derived from experimental data when neglecting interdomain mobility. This distinction between the two domains in the symmetry properties of the "reported" diffusion tensor of Ub$_2$ is similar for both pH conditions, thus suggesting that the data reflect some intrinsic dynamic properties of the system. It is worth mentioning that the alignment tensors derived from residual dipolar couplings (RDCs) measured in Ub$_2$ at pH 6.8 show a similar difference in the apparent rhombicity between the two Ub domains.[8,11] All these data indicate the presence of interdomain dynamics and set their time-scale limits: in order to have an effect on relaxation rates (and hence on the apparent diffusion tensor), these motions must be faster than or comparable to the overall tumbling of Ub$_2$.

Here we use ^{15}N relaxation data to characterize interdomain dynamics leading to the opening of the interdomain interface in di-ubiquitin. To quantify the above-mentioned observations, we considered interdomain dynamics in Ub$_2$ as domain reorientations occurring via interconversion between distinct conformational states of the molecule. The analysis reveals domain reorientations on a ~10-ns time scale that open the Ub/Ub interface in Ub$_2$ thus making the hydrophobic residues available for direct interactions with various chain-recognition factors.

MATERIALS AND METHODS
The Model of Interdomain Motion

The simplest model considered here involves interconversion between two states (ITS) of Ub$_2$ (henceforth called states A and B) characterized by distinct orientations of each domain with respect to some global protein coordinate frame P. These orientations are given by two sets of Euler angles, $\Omega^A = \{\alpha^A, \beta^A, \gamma^A\}$ and $\Omega^B = \{\alpha^B, \beta^B, \gamma^B\}$ for

each domain, and the transitions from A to B and backwards are characterized by the rate constants k_{AB} and k_{BA}, respectively. We assume here that the domain structure and intradomain (backbone) dynamics are the same in both states (as shown in Ref. 8). The overall tumbling of Ub$_2$ is considered fully anisotropic, characterized by the rotational diffusion tensor $\underline{\underline{D}}$.[16] For simplicity, we use the principal axes frame of this tensor as the global protein coordinate frame P; motion of each domain is then described as its reorientation with respect to P.

To include the interdomain dynamics, we considered the orientation of a given internuclear vector (^{15}N—^{1}H) with respect to the static magnetic field $\vec{B}_o$ as a set of subsequent rotational transformations (Supplementary Figure): from the laboratory frame L (aligned with $\vec{B}_o$ to the diffusion tensor frame P, then to the coordinate frame D for each domain (e.g., PDB coordinate frame), then to the residue-specific frame R associated with the average (over the time interval longer than the correlation time of the local motion) orientation of a given NH-vector within each individual domain, and, finally, to the instant frame I attached to the NH-vector. The relaxation-relevant correlation function can then be written in the following general form:

$$C(t) = \langle D_{q,0}^{(2)*}(\Omega_{L \to I}^0) D_{q,0}^{(2)}(\Omega_{L \to I}^t) \rangle$$

$$\cong \sum_{m=-2}^{2} \sum_{n=-2}^{2} \sum_{k=-2}^{2} \sum_{l=-2}^{2} \sum_{s=-2}^{2} \sum_{h=-2}^{2} \langle D_{q,m}^{(2)*}(\Omega_{L \to P}^0) D_{q,n}^{(2)}(\Omega_{L \to P}^t) \rangle$$

$$\times \langle D_{m,k}^{(2)*}(\Omega_{P \to D}^0) D_{n,l}^{(2)}(\Omega_{P \to D}^t) \rangle$$

$$\times D_{k,s}^{(2)*}(\Omega_{D \to R}^0) D_{l,h}^{(2)}(\Omega_{D \to R}^0) \langle D_{s,0}^{(2)*}(\Omega_{R \to I}^0) D_{h,0}^{(2)}(\Omega_{R \to I}^t) \rangle \quad (1)$$

where $D_{m,n}^{(2)}$ are components of the Wigner rotation matrix, Ωs are the Euler angles for the corresponding rotations (as

indicated by the subscripts), and the angular brackets represent averaging over the corresponding processes of motion. The interdomain motion affects the second step, $P \to D$; the corresponding term in $C(t)$ can be cast as:

$$\langle D_{m,k}^{(2)*}(\Omega_{P \to D}^0) D_{n,l}^{(2)}(\Omega_{P \to D}^t) \rangle = p_A(p(A|A,t) D_{m,k}^{(2)*}(\Omega^A) D_{n,l}^{(2)}(\Omega^A)$$
$$+ p(A|B,t) D_{m,k}^{(2)*}(\Omega^A) D_{n,l}^{(2)}(\Omega^B))$$
$$+ p_B(p(B|A,t) D_{m,k}^{(2)*}(\Omega^B) D_{n,l}^{(2)}(\Omega^A)$$
$$+ p(B|B,t) D_{m,k}^{(2)*}(\Omega^B) D_{n,l}^{(2)}(\Omega^B)) \quad (2)$$

Here $p_A = k_{BA}/(k_{AB} + k_{BA})$ and $p_B = k_{AB}/(k_{AB} + k_{BA})$ are the equilibrium occupation probabilities for states A and B, respectively; $p(A|A,t) = p_A + p_B e^{-(t/\tau_{ITS})}$ and $p(B|B,t) = p_B + p_A e^{-(t/\tau_{ITS})}$ are the conditional probabilities to find the system at time t in the same state (A or B) as at $t = 0$; and $p(A|B,t) = p_B(1 - e^{-(t/\tau_{ITS})})$ and $p(B|A,t) = p_A(1 - e^{-(t/\tau_{ITS})})$ are the conditional probabilities to find the system in a different state (B or A) at time t. In these equations, we introduced characteristic interconversion time τ_{ITS}, which is the reciprocal of the rate of interconversion $K = k_{AB} + k_{BA}$ between the two states. (Note a simple relationship between the rate constants and τ_{ITS}: $k_{AB} = (1 - p_A)/\tau_{ITS}$; $k_{BA} = p_A/\tau_{ITS}$). The correlation functions describing the overall $(L \to P)$ and "model-free" local backbone $(R \to I)$ dynamics can be found in Woessner[16] and Lipari and Szabo,[17] respectively. The angles $\Omega_{D \to R}$ specifying the average orientation of the NH vector in the coordinate frame of the corresponding domain are assumed time-independent. A detailed description of the model will be published elsewhere (Ryabov and Fushman, forthcoming).

Our rationale for choosing the interconversion-between-two-states model is based on the observation of a well-defined interdomain interface in Lys48-linked Ub$_2$,[11] indicating the existence of a definitive conformation of the chain, predominantly populated at pH 6.8 and higher. This is different from the case of calmodulin[18–20] where there is no preferred interdomain orientation, thus "extended model-free" or "wobbling-in-a-cone" models considering a continuum of available interdomain conformations were adequate. These models would not be adequate for interdomain motions in Ub$_2$ because they do not allow assigning arbitrary, unequal occupation probabilities to different interdomain orientations. The ITS model of interdomain dynamics provides a structurally detailed although still simple description of domain mobility in a two-domain system.

Equation 1 assumes that the overall tumbling of Ub$_2$, the domain mobility within the molecule, and local dynamics within each Ub unit are all *statistically independent* of each other (hence the separation of the corresponding correlation functions). While obvious for the local dynamics that usually are fast (1–100 ps) and, therefore, average out on the time scale ($\sim$10 ns) relevant for the overall and interdomain motions, this assumption is less intuitive when applied to the latter motions, especially if their characteristic times are not significantly different from each other. The overall tumbling is considered decoupled from the interdomain dynamics, in the sense that there is no causality between these two modes of motion. (Note that essentially the same assumption was made when applying the "extended model-free" model to interdomain dynamics in calmodulin.[18]) While clearly an approximation, this assumption is expected to be accurate, for example, in the case when spherical-shape domains reorient with respect to each other while preserving the relative positions of their centers of mass in a molecule: such motion will not change the overall shape nor the hydrodynamic properties (diffusion tensor) of the whole molecule. In fact, the picture of interdomain motions in Ub$_2$ [Fig.1(a–d)] obtained from the analysis below bears a certain resemblance to this simple scheme. A more accurate treatment should include causality relationship (coupling) between the interdomain and overall dynamics and could, in principle, be obtained from the corresponding Smoluchowski equation. In this regard, the emerging mode-coupling approaches[21–23] are promising, although the exact physical meaning of the resulting picture of protein dynamics obtained when applying these ideas to particular proteins[24,25] remains to be understood. Interestingly, however, as shown below, the simple model considered here is capable of capturing the essential features of domain dynamics in Ub$_2$.

Note also that the assumption of statistical independence of the overall and interdomain motions is a separate one from the ability to accurately and independently extract their characteristics from the available experimental data. As a matter of fact, the interdomain mobility in Ub$_2$ happens to be in the same time range as the overall tumbling (see below), which necessarily limits the precision of the derived rates of interconversion.

It is worth pointing out that the ITS model proposed here is rather general in the sense that no a priori assumption is being made about the relationship between the characteristic time scales of the interconversion and the overall tumbling. Therefore, this model is capable of covering a range of situations, from fast ($\tau_{ITS} \ll \tau_c$) to intermediate ($\tau_{ITS} \sim \tau_c$, as in the case of Ub$_2$, see below) to slow ($\tau_{ITS} \gg \tau_c$) interconversion and thus allows a continuous adjustment of the interconversion time in order to properly fit the experimental data.

NMR Data

The NMR data used in this study comprise ^{15}N relaxation rates (R_1 and R_2) and steady-state heteronuclear ^{1}H—^{15}N NOEs, as well as relaxation rate enhancement caused by site-specific spin-labeling. All these parameters were measured in both Ub domains in Ub$_2$ at 14.1 Tesla and 24°C as reported earlier in Fushman et al.[8] and Varadan et al.[11] Throughout this report, the Ub unit that carries the free C-terminus is defined as the "proximal" domain, while the other Ub domain in Ub$_2$ is called "distal." Thus, the two Ub molecules in Ub$_2$ are linked via an isopeptide bond between the C-terminal Gly76 of the distal Ub and Lys48 of the proximal Ub. Ub$_2$ chains ^{15}N-labeled at the proximal or distal Ub domain were assembled from recombinant Ub molecules (unlabeled and ^{15}N-labeled) using segmental isotope labeling strategy.[11]
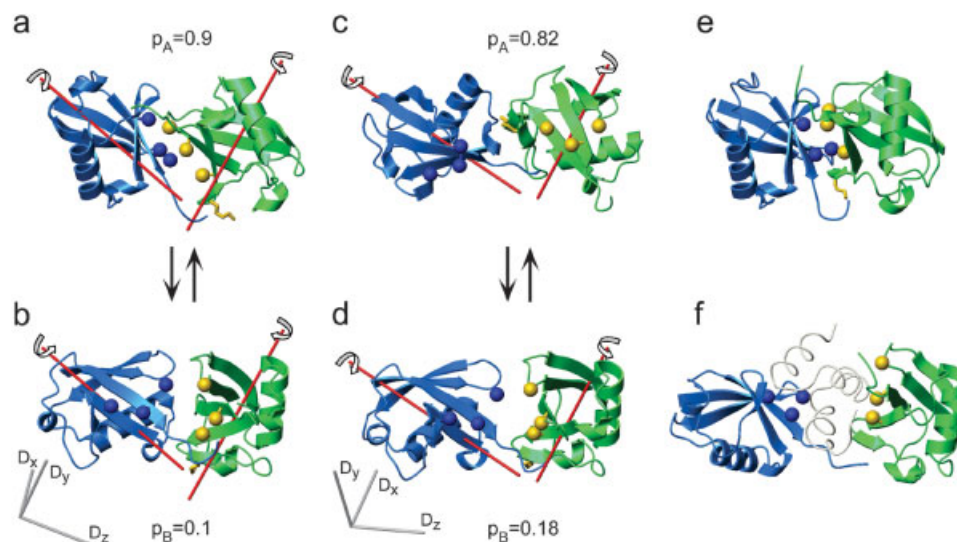
Fig. 1. Conformations of the Lys48-linked Ub$_2$ in the states A and B at pH 6.8 (**a,b**) and pH 4.5 (**c,d**). Also shown, for comparison, are (**e**) the crystal structure[12] of Ub$_2$ and (**f**) the solution structure of the Ub$_2$ complex with the UBA2 domain of hHR23A.[15] The distal domain is colored blue, the proximal is green. Rods represent the principal axes of the overall diffusion tensor (gray) and the rotation axes (A↔B) for each domain (red). The curved arrows indicate the direction of rotation towards the other state. Only interdomain orientation, not the distance, is available from the current analysis: the Ub domains in a–d are positioned somewhat arbitrarily with respect to each other, such as to bring the (flexible) C-terminus of the distal Ub in close proximity to Lys48 of the proximal Ub and to preserve some resemblance to domain positioning in the crystal structure. The predicted diffusion tensors for all resulting structures are close to the experimentally observed diffusion tensors (Supplementary Table I). The location of hydrophobic patch residues (Leu8-Ile44-Val70) is shown in ball-and-stick (C$_\beta$ atoms, colored blue for the distal and gold for the proximal). The side chain of Lys48 (proximal Ub) is shown in stick (gold). The occupation probabilities for each Ub$_2$ conformation are indicated. In f, the UBA2 domain is shown as a backbone ribbon (ivory). These drawings here and in Figure 4 were made in MolMol.[36]
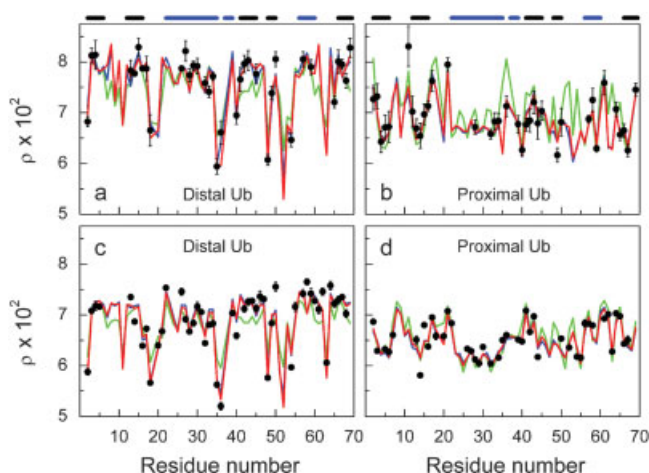

Fig. 2. The quality of fit of the experimental ^{15}N relaxation data at (**a,b**) pH 6.8 and (**c,d**) pH 4.5 using various approaches considered here. The measured values of ρ (Eq.3) are shown as circles. The lines represent the results of fitting, colored as follows. Red corresponds to simultaneous fit of both Ub domains in Ub$_2$ using the ITS model, i.e., combining anisotropic overall diffusion with the interconversion between two states; green is for the simultaneous fit of both domains assuming anisotropic diffusion but ignoring the interdomain motion; and blue represents the anisotropic diffusion model applied to each domain separately. The lines show prediction for all residues in Ub$_2$, while the symbols indicate only those residues that were included in the fit. The horizontal bars on the top indicate elements of the secondary structure of Ub (black for β-strands, blue for the helices). Note the difference in the overall levels of ρ between the two Ub domains, which makes it practically impossible to fit well the data for both domains simultaneously if the interdomain mobility is ignored.
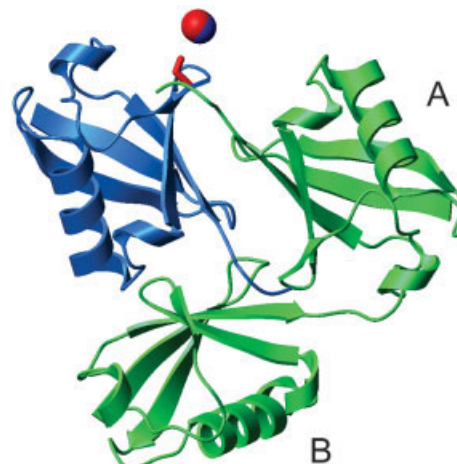

Fig. 4. Validation of the Ub$_2$ conformations at pH 6.8 using site-specific spin labeling. Shown are the structures of Ub$_2$ in the states A and B, superimposed by the distal domains, and the location of the spin label (red and blue spheres) reconstructed from the measured signal attenuations in both Ub domains. Red sphere corresponds to the analysis taking into account both Ub$_2$ conformations, while the blue sphere represents the results for the closed conformation only. Also shown (in red stick) are the C$_\alpha$–C$_\gamma$ atoms of the side chain of Lys48 of the distal Ub; this residue was mutated to a cysteine in this study that served as a SL attachment site. The distal domain is colored blue, the proximal is green; "A" and "B" indicate the positions of the proximal domain in the states A and B, respectively. The orientation of Ub$_2$ corresponding to state A is similar to that in Figure 1(a).

TABLE II. Characteristics of the Overall Rotational Diffusion Tensor and Interdomain Mobility for Lys48-Linked Ub₂ at Neutral and Acidic Conditions†

pH	D_x[a]	D_y[a]	D_z[a]	τ_{ITS}[b]	p_A[c]	Domain	α^{A}[d]	β^{A}[d]	γ^{A}[d]	α^{B}[d]	β^{B}[d]	γ^{B}[d]
						Proximal	218	109	140	203	110	72
6.8	1.53	1.73	2.20	9.3	0.90		(35)	(11)	(4)	(38)	(9)	(8)
	(0.32)	(0.06)	(0.08)	(4.8)	(0.06)	Distal	91	58	321	156	96	356
							(28)	(7)	(19)	(33)	(38)	(33)
						Proximal	147	112	322	191	122	45
4.5	1.61	1.71	2.20	31.9	0.82		(30)	(16)	(8)	(25)	(14)	(13)
	(0.13)	(0.06)	(0.06)	(9.8)	(0.06)	Distal	213	80	350	151	51	328
							(24)	(8)	(12)	(29)	(20)	(23)

†Numbers in the parentheses represent estimated uncertainties in the parameters.
[a]Principal components, D_x, D_y, and D_z, of the overall diffusion tensor, in 10^7 s^{-1} (ordered as $D_x \leq D_y \leq D_z$).
[b]Characteristic time constant for the interconversion between the two states, $\tau_{ITS} = 1/K$, in 10^{-9} s.
[c]Occupation probability for the more populated state (this state is called state A); the occupation probability for state B is $p_B = 1 - p_A$.
[d]The Euler angles, in degrees, specifying for the states A and B the orientation of the PDB frame for each Ub domain with respect to the reference frame of the overall diffusion tensor. Protein atom coordinates were from the solution structure of monomeric Ub (PDB entry 1D3Z, model 1).[35] The use of these coordinates for the individual domains in Ub₂ has been validated by RDC measurements.[8] The original Ub coordinates were rotated by {90°, 90°, 180°} to avoid having β ≈ 0 or 180° when the angles α and γ cannot be accurately separated.

The relaxation data were collected at pH 4.5 and 6.8. Spin-labeling experiments were performed at pH 6.8. Here, a paramagnetic spin label (SL), (1-oxyl-2,2,5,5-tetramethyl-3-pyrroline-3-methyl)methanesulfonate, was covalently attached to a single Cys residue in Ub₂ (distal domain, K48C Ub) and the relaxation rate enhancement (signal attenuation) caused by the SL was monitored in both Ub domains. The details of these measurements are presented elsewhere.[8,26]

Relaxation Data Analysis

The analysis of ^{15}N relaxation data was focused on the ratio

$$\rho = \frac{R_1'}{2R_2' - R_1'}, \qquad (3)$$

where R_1' and R_2' are the modified rates of longitudinal and transverse ^{15}N relaxation, respectively (see, e.g., Ref. 4): $R_1' = R_1[1-1.249|\gamma_N/\gamma_H|(1 - \text{NOE})]$; $R_2' = R_2 - 1.079|\gamma_N/\gamma_H|R_1(1 - \text{NOE})$. This modification corresponds to subtraction of the contributions to relaxation rates from the high-frequency components of the spectral density. The quantity ρ is independent of the site-specific variations in the ^{15}N chemical shift anisotropy and, for protein core elements, of the local backbone motion.[8]

The experimental data for both Ub domains at a given pH were analyzed simultaneously. In total, 71 amides included in the analysis at pH 6.8 belong to residues 2–6, 11–17, 21, 28, 32–34, 36, 39–45, 49, 50, 57–59, 61, 64–67, and 69 in the proximal and 2–4, 13–18, 26–30, 32–36, 40–43, 45, 48–50, 54, 57, 59, 65–69 in the distal Ub. The 91 residues analyzed at pH 4.5 were 2, 3, 5–7, 13–18, 20–22, 26–30, 32, 34–36, 39–44, 50, 52, 54–58, 61–67 (proximal Ub) and 2–5, 13, 14, 16–18, 20–22, 26–36, 39, 40, 42–50, 54, 55, 57–68 (distal Ub). The fitting parameters (17 altogether) included the principal values (D_x, D_y, D_z) of the diffusion tensor, the characteristic interconversion time τ_{ITS} (=1/K), and the occupation probability for one of the two states (these five parameters were consid-

ered the same for both domains) and domain-specific sets of Euler angles Ω^A and Ω^B describing the orientations of each domain in the two states.

In a control fit, the interdomain mobility was turned off by setting $1/k_{BA} = 0$ (hence $p_A = 1$), which resulted in a single (static) conformation, hence a single orientation per domain. Note that this analysis differs from the previous approach[8,11] (Table I) where the overall diffusion tensor of Ub₂ was determined for each domain separately.

The fitting parameters were obtained by minimizing the target function:

$$\chi^2 = \sum_{k=1}^{N} \left(\frac{\rho_k^{\text{exp}} - \rho_k^{calc}}{\sigma_k} \right)^2, \qquad (4)$$

where N is the total number of NH vectors included in the analysis and σ_k denotes the experimental error in ρ_k for residue k. The value of ρ^{exp} is directly derived from the measured relaxation parameters (Eq.3), while ρ^{calc} is calculated by incorporating Eqs.1 and 2 into regular expressions (see, e.g., Ref. 27) for spin-relaxation rates. The minimization of χ^2 was performed using an in-house program based on a simplex algorithm. Multiple runs with various starting conditions were performed, to assure that the solution corresponds to a global minimum. The confidence intervals in the fitting parameters were estimated using the bootstrap method,[28] by applying the same analysis to computer-generated synthetic sets of data. Each data set was generated by replacing 37% of randomly chosen data points with the duplicates of the randomly selected points from the original set of experimental data. This procedure was performed for both domains independently and simultaneously, such that each synthetic data set contained 37% substituted points for the distal domain and the same percent of points for the proximal domain. The confidence intervals obtained from statistical analysis of 200 data sets are shown in Table II.

Analysis of Signal Attenuations Caused by Spin Labeling

The signal attenuation caused by the spin label was measured as the ratio, I_{ox}/I_{red}, of NMR signals in ^{15}N—^1H HSQC spectra recorded with the spin-label in the oxidized (paramagnetic) and reduced states, as detailed elsewhere.[8,26] The position of the spin label was reconstructed from simultaneous analysis of signal attenuations observed in the amide groups from both Ub domains. This was done by a simplex-based three-dimensional search that minimized the difference between the experimentally measured and predicted values of I_{ox}/I_{red}. For this search, the Ub_2 conformations shown in Figure 1(a,b) were superimposed by their distal domains, and for each location of the SL the signal attenuation was calculated as follows:

$$I_{ox}/I_{red} = exp(-t\Delta R_{2para}), \qquad (5)$$

where t is the total experimental time when the amide proton magnetization is in the transverse plane and undergoing paramagnetic relaxation (see, e.g., Ref. 29), and $\Delta R_{2para} = R_{2ox} - R_{2red}$ is the relaxation rate enhancement. The value of ΔR_{2para} depends on the distance r between the nucleus under observation and the unpaired electron of the SL as[30]:

$$\Delta R_{2para} = \frac{1}{20}\,\gamma_H^2 g_e^2 \beta_e^2 \left(4\tau_c + \frac{3\tau_c}{1+\omega_H^2\tau_c^2}\right)\left\langle\frac{1}{r^6}\right\rangle, \qquad (6)$$

where τ_c is the rotational correlation time of the molecule, γ_H and ω_H are the ^1H gyromagnetic ratio and resonance frequency, g_e is the electronic g-factor, and β_e is the Bohr magneton. Here the angular brackets represent averaging over the nucleus-SL distances in the states A and B (r_A and r_B, respectively):

$$\left\langle\frac{1}{r^6}\right\rangle = \frac{p_A}{r_A^6} + \frac{p_B}{r_B^6}, \qquad (7)$$

which reflects the fact that the interconversion between the two states occurs on a much faster time scale than nuclear spin relaxation.

RESULTS AND DISCUSSION
Interdomain Dynamics in Di-Ubiquitin

We applied the ITS model to ^{15}N relaxation data measured for backbone amides in Ub_2 at pH 6.8 and 4.5. In total, 71 amide groups belonging to the Ub core in both domains were analyzed for pH 6.8 and 91 for pH 4.5; residues in the flexible loops/termini and those affected by conformational exchange broadening were excluded from the analysis. The derived characteristics of the overall and interdomain dynamics and the relevant structural parameters are presented in Table II. The resulting conformations of Ub_2 are depicted in Figure 1(a–d); the quality of the fit is shown in Figure 2.

The interconversion between states A and B at a given pH can be represented as a rotation of each domain about a certain axis, as indicated in Figure 1. The corresponding rotation angles are 65° and 87° for the proximal and distal

Ub, respectively, at pH 6.8 and 73° and 79° at pH 4.5. Notably, the orientation of the rotation axes is similar for both pH values (Fig. 1): in both domains these axes go through the linkage region, consistent with its expected role as a pivot point in the interdomain reorientation. Interestingly, however, the axes of rotation differ between the two domains. This likely reflects the inequivalence of the Ub domains in the way they are linked to each other: the distal domain is connected via its C-terminus (unstructured and flexible on the ns time scale), while Lys48, the linkage site on the proximal Ub, is located in a short although relatively rigid β-strand.[8] These results explain the apparent asymmetry between the overall diffusion tensors derived for the two domains when neglecting the interdomain motion (Table I). Indeed, the rotation axis of the distal domain is oriented close to the z-axis of the diffusion tensor (the tilt angle is 38° at pH 6.8, 29° at pH 4.5), hence higher apparent anisotropy of the tensor as the domain's rotation adds to the apparent D_z value. For the proximal domain, on the contrary, the rotation axis is oriented almost perpendicular (99° at pH 6.8, 90° at pH 4.5) to the z-axis of the diffusion tensor of Ub_2. The domain's rotation will average D_z with the perpendicular components (primarily D_y), resulting in smaller apparent anisotropy and higher rhombicity of the tensor.

There is a good agreement between the principal values of the diffusion tensor of Ub_2 at both pH values (Table II). Because the predominant Ub_2 conformations at the two pH values are very different [Fig. 1(a,c)], this result indicates that different orientations of the Ub domains in Ub_2 do not significantly affect the principal values of the overall diffusion tensor, which a posteriori justifies the approximation that the interdomain mobility in Ub_2 is decoupled from the overall tumbling. This conclusion is also supported by the results of hydrodynamic calculations (see Supplementary Table 1) that give very similar principal values of the overall diffusion tensor for both Ub_2 conformations at each pH [Fig. 1(a–d)].

As expected, the characteristic time of interconversion, $\tau_{ITS} = 9.3\pm4.8$.ns at pH 6.8 is comparable to the overall tumbling time ($\tau_c = 9.2 \pm 0.7$ ns). The interconversion at pH 4.5 is slightly slower than the overall tumbling (31.9 $\pm$ 9.8 ns versus 9.1 $\pm$ 0.3 ns). The large estimated uncertainty in the interconversion rate reflects the fact that it is close to the rate of the overall tumbling, which prevents accurate separation of the contributions from these two motions in the error analysis. This imprecision in the interconversion rates in Ub_2, however, seems to have little effect on the rest of the fitting parameters (Table II) which turn out to be in good agreement with other NMR and structural data (see below).

The back-calculated relaxation parameters are in good agreement with the experimental data (Fig. 3). Because a model with more fitting parameters usually provides a better fit, in order to validate the inclusion of the interdomain motion, we compared the residuals of fit obtained using the ITS model with the results of a global fit of the same data assuming that Ub_2 exists in a single conformation and there is no domain motion (see Materials and
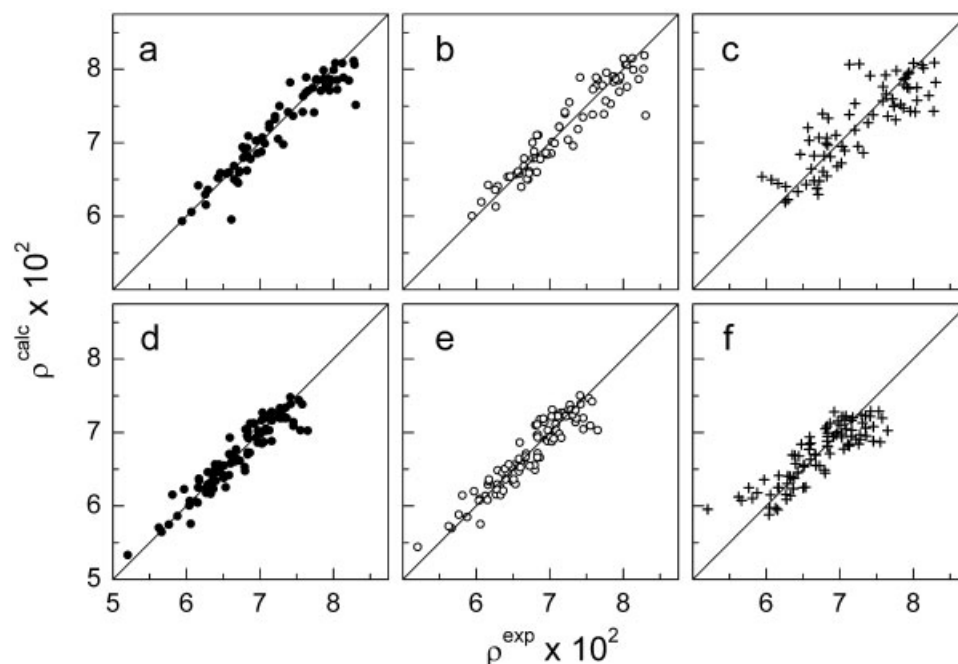
Fig. 3. The agreement between experimental (ρ^{exp}) and back-calculated (ρ^{calc}) ^{15}N relaxation data (ρ, Eq.3) at (**a–c**) pH 6.8 and (**d–f**) pH 4.5 for various approaches considered here. Shown are data for (a, d) global fit using the ITS model (solid circles), (b, e) data fit for each domain separately using anisotropic diffusion tensor model (open circles), and (c, f) global fit ignoring interdomain motion (crosses). The Pearson's correlation coefficient between ρ^{exp} and ρ^{calc} is 0.952 (a), 0.946 (b), 0.84 (c), 0.942 (d), 0.938 (e), and 0.86 (f).

Methods). Neglecting the interdomain dynamics significantly worsened the fit [Figs. 2 and 3(c,f)], resulting in a 3.2-fold increase in χ^2 per degree of freedom (from 1.69 to 5.47) at pH 6.8; the corresponding increase in χ^2 at pH 4.5 was 2-fold. Based on the statistical F-test,[28] this indicates a very low probability ($5 \cdot 10^{-12}$ for pH 6.8 and $2 \cdot 10^{-9}$ for pH 4.5) that the better fit obtained for the ITS model occurred by chance. These results thus provide a statistical validation for the inclusion of the interdomain dynamics. It is also worth noting that the quality of the global fit using the ITS model was similar or even slightly better than when analyzing the data for each Ub domain separately [Figs. 2, 3(b,e)]; in the latter case, for example, at pH 6.8 the χ^2 per degree of freedom was 2.76 and 1.16, for the distal and proximal Ub, respectively.

Agreement With Other NMR Data
Chemical shift perturbation data

The occupation probabilities for the two states, $p_A = 0.9$ and $p_B = 0.1$ for pH 6.8, are in excellent agreement with the values ($p_A \geq 0.85$, $p_B \leq 0.15$ at pH 6.8) estimated earlier from pH titration data.[11] Also the interdomain orientations obtained here agree well with the chemical shift perturbation data.[11] The closed conformation (state A) at pH 6.8 [Fig.1(a)], in which the hydrophobic patches on both Ub domains face each other, is fully consistent both with the results of chemical shift perturbation mapping at these conditions[11] and with the key role of these residues in the formation of the Ub/Ub interface [Fig. 1(e)]. The Ub$_2$ conformations at pH 4.5 [Fig.1(c,d)] are also

consistent with the chemical shift data that indicate the absence of a direct contact between these residues at acidic pH.

Validation using paramagnetic spin labeling

To independently validate the Ub$_2$ conformations derived at pH 6.8 [Fig. 1(a,b)], we turned to signal attenuations observed in Ub$_2$ as a result of site-specific spin labeling of the distal domain. An unpaired electron of the spin label causes paramagnetic relaxation rate enhancement resulting in broadening of resonances (hence signal attenuation) for those nuclei that are close in space to the spin label. The attachment of the SL to Cys48 in the distal Ub (K48C mutant) resulted in signal attenuations in both domains, thus verifying the predominantly closed conformation of the chain at pH 6.8. To quantify these observations, we reconstructed the location of the SL relative to Ub$_2$ molecule in the three-dimensional space using relaxation rate enhancements observed in both Ub domains (see Materials and Methods). This analysis positioned the unpaired electron of the SL (Fig. 4) at a distance of 6.2 Å from C_α and 5.6 Å from C_β of residue 48 in the distal Ub (the site of SL attachment), in good agreement with its expected location (about 5–7 Å from C_β). A similar position of the spin label was obtained when considering only the closed conformation of Ub$_2$. This can be explained by the fact that in the open conformation at pH 6.8 (state B) the proximal domain is positioned far away from the SL (Fig. 4), hence the data are not sensitive enough to the exact location of this domain in the open state. To explore the

sensitivity of the data to occupation probabilities of the two conformations, the position of SL was also calculated assuming that only the open conformation is populated ($p_B = 1$). This resulted in an unrealistically long distance (16.8 Å) from C_α, thus confirming that the open conformation is not the predominant one under these conditions. Accurate determination of p_A from these data, however, was not possible. For example, assuming equal probabilities for the two states placed the SL at a position shifted by 1.3–1.6 Å from those in Figure 4, yet close enough (5.5 Å) to C_α, which could also be acceptable, as the exact location of the SL is not well defined due to local mobility. Although this analysis does not allow accurate validation of the open conformation of Ub_2 and its occupation probability, we nevertheless can conclude that the Ub_2 conformations obtained at pH 6.8 do not contradict our spin-labeling data, and, moreover, the closed conformation of Ub_2 agrees well with these data.

pH Dependence of the Ub_2 Conformations

As mentioned earlier, NMR data[11] indicate the disappearance of a defined Ub/Ub interface as pH is titrated from 7.5 to 4.5. The Ub/Ub interface is stabilized by a balance between the hydrophobic interaction of the two domains and their electrostatic repulsion due to positively charged side chains surrounding the hydrophobic patches on both Ub domains. Lowering the pH from 6.8 to 4.5 is expected to cause the protonation of His68 (pKa = 5.5[31]) adjacent to the hydrophobic patch on both Ub units. The accompanying increase in the Coulomb repulsion of the two domains is perhaps the reason that the closed state [Fig. 1(a)] becomes energetically unfavorable at low pH. From the ratio of the occupation probabilities of states A and B, the difference in their Gibbs free energies is $\Delta G \equiv G_A - G_B \approx -5.5$ kJ/mol (pH 6.8) and -3.8 kJ/mol (pH 4.5), where the lower-energy state (state A) corresponds to the closed conformation at pH 6.8 [Fig.1(a)] and the open one at pH4.5, shown in Figure 1(c). In this regard, the picture of interconverting Ub_2 conformations obtained here [Fig.1(a–d)] is more complex than a simple, seemingly intuitive model in which the (open and closed) limiting states would be the same at both pH values and only their relative population would change with pH. A change in the nature of the Ub/Ub interaction from hydrophobic attraction to electrostatic repulsion not only will affect the occupation probabilities of the two states, but will also alter the structure of the "closed" conformation, because the interdomain contact observed at neutral pH [Fig.1(a,e)] will be energetically unfavorable at a lower pH. It should be mentioned here that a well-defined interdomain orientation in the open conformation (state A) at pH 4.5, despite the apparent lack of specific Ub/Ub interactions, likely reflects the simplicity of the two-state model used in this study. Further refinement of the model of interdomain dynamics, for example, by allowing wobbling-type motions in the "open" state, might be necessary to improve the representation of the open conformations.

It is worth noting the similarity between the Ub_2 conformations in the state B at both pH [Fig. 1(b,d)]. One might speculate that these conformations could correspond to some stable intermediate in the Ub_2 transition from the predominantly closed, hydrophobic-interface conformation [Fig. 1(a)] at physiological conditions to the no-interface conformation [Fig. 1(c)] dominant at acidic pH. Such a transition would be consistent with the directions of domain rotations. Further studies are necessary to test this hypothesis.

Interdomain Motions on a Slower Time Scale

A complete picture of interdomain dynamics in Ub_2 should include domain motions that are significantly slower than the overall tumbling. For example, conformational exchange was detected in several amides located at the Ub/Ub interface,[11] thus indicating the presence of interdomain motions on a time scale from 50 to 500 μs.[8] The fact that the conformational exchange contributions are absent at pH 4.5, where the Ub/Ub interface is not formed [Fig. 1(c,d)], suggests that they likely reflect some interdomain dynamics (perhaps domain "bumping" into each other) related to the closing/opening of the interface [Fig. 1(a,b)]. Unfortunately, the actual amplitudes of such motions cannot be reliably extracted from the measured conformational exchange.

Interestingly, however, there is a good agreement between the solution conformations of Ub_2 obtained from rotational diffusion and alignment tensor data (at pH 6.8) under the assumption that interdomain motions can be neglected.[8,11,13] While the rotational anisotropy and sterically induced alignment are both determined by the shape of the protein,[32,33] they probe domain dynamics in different time-windows: ps-ms for residual dipolar couplings and ps-ns for ^{15}N relaxation measurements. Therefore, if significant interdomain motions slower than the overall tumbling (yet fast enough to average the RDCs) were present, these would affect RDCs but not relaxation rates, and thus average the alignment tensor differently from the diffusion tensor. The agreement between the Ub_2 conformations derived from these two physically distinct characteristics is remarkable[8,11] and indicates that conformational averaging (due to interdomain dynamics in Ub_2) primarily occurs on the time scale comparable to or faster than the overall tumbling. This also suggests that domain motions reflected in the conformational exchange in Ub_2 are of relatively small amplitude, such that they do not significantly affect the RDC data.

Comparison with a Slow-Interconversion Model

As mentioned above (see Materials and Methods), the ITS model can also describe the situation when the interconversion is much slower than the overall tumbling, yet faster than spin-relaxation. In this case, the dynamic nature of the process of interconversion can be neglected, and the apparent relaxation rate should be a population average of the corresponding rates for the two conformations. The corresponding equations for the spectral densities can be obtained directly from Eqs.1–2 (and Fourier transform thereof) by simply setting $\tau_{ITS} \gg \tau_c$. In the general analysis presented above, the rate of interconver-

sion was not forced to assume any particular fixed value. However, because it turned out that $\tau_{ITS} > \tau_c$ at pH 4.5, we also analyzed the data by forcing the ITS model into the slow interconversion regime. This was achieved by setting $\tau_{ITS} = 1$ s. Using the values from Table II for the rest of the parameters resulted in a significantly worse agreement between the experiment and the model (e.g., a 40-fold increase in χ^2). However, when the ITS model parameters (except τ_{ITS}) were allowed to float, the agreement improved dramatically, and at pH 4.5 this model was able to fit the experimental data almost as well as the full model. The latter reflects the fact that when reorientational motion (in this case, interconversion) is slower than the overall tumbling, its effect on the spin Hamiltonian is reduced, hence the relaxation data become less sensitive to the actual time constant characterizing this motion. However, a detailed analysis of the results of these fits shows that the fitting procedure redistributed the impact of interdomain dynamics to other adjustable parameters. For example, the occupation probabilities obtained from the fit were almost equal for both Ub_2 conformations ($p_A = 0.60$, $p_B = 0.40$ at pH 6.8 and $p_A = 0.54$, $p_B = 0.46$ at pH 4.5), which contradicts the experimental data on chemical shift perturbations[11] that indicate a predominantly closed conformation at pH 6.8 and a predominantly open one at pH 4.5. Although a simple substitution of interdomain dynamics with a population average cannot properly describe the experimental data for Ub_2, this feature of the ITS model might turn useful in applications to other multidomain systems where the interconversion is much slower than the overall tumbling.

Comparison With the "Extended Model-Free" Model

As mentioned above, the "extended model-free" approach (EMFA) is not expected to adequately describe the interdomain motions in Ub_2. In order to verify this conclusion, we analyzed the data using the "extended model-free" approach, implemented in a similar way as in Baber et al.[18] In the original analysis[18] of the relaxation rates, the order parameters of local motion, assumed to be uniform throughout each domain, were included in the fit. Because we analyze the ratio ρ of relaxation rates (Eq. 3), which is not sensitive to the order parameters of local backbone motion, these were set to 1. Note also that our analysis was not restricted to axially symmetric diffusion tensor. Fitting using EMFA resulted in a 2-fold increase (compared to the ITS model) in the residuals of fit per degree of freedom at both pH values and in a worse correlation between the experimental and back-calculated data (Pearson's correlation coefficient was 0.89 vs. 0.95 for pH 6.8 and 0.86 vs. 0.94 for pH 4.5 data). Moreover, in contrast to the ITS model, EMFA produced physically unreasonable values of the fitting parameters (Supporting Table II). Here the overall tumbling time of Ub_2 was 17 ns (pH 6.8) and 11 ns (pH 4.5) and the squared order parameters associated with the interdomain mobility were 0.02 for the distal and 0.3 for the proximal domain at pH 6.8 and 0.2 and 0.56, respectively, at pH 4.5.

Biological Significance: Agreement With the Structural Data

As shown above, despite the obvious simplicity of the proposed ITS model, it proved capable of describing experimental chemical shift perturbations and ^{15}N relaxation data. Moreover, the resulting interdomain orientation in the "closed" state [Fig. 1(a)] positions both Ub domains such that their hydrophobic patches are capable of forming a hydrophobic interface similar to that seen in the crystal structure of Ub_2 [Fig. 1(e)],[12] which likely captured a snapshot of Ub_2 in the closed conformation. Figure 1(a) is also consistent with the docked structure models of Ub_2 obtained based on chemical shift perturbations alone and in combination with RDC data.[13] Note that these latter structures were obtained independently of the ^{15}N relaxation data and neglecting the interdomain motion. The "closed" Ub_2 conformation is also similar to those obtained by aligning the diffusion tensors or the alignment tensors derived from the analysis of the two Ub domains separately and neglecting domain dynamics.[8,11]

The "open", binding-competent state of Ub_2 at pH 6.8 [Fig. 1(b)] is weakly populated and, therefore, less well sampled compared to the "closed" state. Interestingly, however, the orientation of the two domains in the open conformation obtained here is similar to that in the ligand-bound state of Ub_2 [Fig. 1(f)].[15] The small differences between Figure 1(b) and (f) could reflect the simplicity of the ITS model but might also be caused by the ligand binding that could drive Ub_2 away from its open conformation in the unbound state. Ligand-induced changes in the interdomain orientation are not unexpected, and have previously been observed by NMR (e.g.,[4]).

In view of all these factors, the similarity between the two conformations of Ub_2 determined here and those obtained by structural methods is remarkable and suggests that the simple ITS model is capable of capturing some essential features of interdomain conformations and dynamics in di-ubiquitin. A more refined structural picture of the interconverting states could be obtained by including additional information, for example, from chemical shift perturbations and residual dipolar couplings; this work is currently in progress.

CONCLUSIONS

Our analysis of ^{15}N relaxation data revealed both the structural and dynamic characteristics of domain motion in Lys48-linked Ub_2 chain. Despite the simplicity of the applied model of interdomain dynamics, these results are in good agreement with the chemical shift perturbation and spin-labeling data and provide the first glimpse at the domain motions and equilibrium conformations in Ub_2 at near-physiological conditions. Moreover, the closed and open conformations of Ub_2 resemble those observed in Ub_2 crystals and in the Ub_2/UBA complex, respectively. These data indicate that the relative orientation of the two domains in Ub_2 fluctuates with an amplitude that could be sufficient for opening the interface at physiological pH, thus allowing various chain-recognition factors direct access to the functionally important hydrophobic residues in

ubiquitin. These results provide, for the first time, insights into the motional processes essential for molecular recognition events in polyubiquitin signaling. The proposed mechanism of interdomain mobility is quite general and could be of relevance to other multidomain systems.

ACKNOWLEDGMENTS

REFERENCES

1. Sicheri F, Kuriyan J. Structures of Src-family tyrosine kinases. Curr Opin Struct Biol 1997;7:777–785.
2. Pickford AR, Campbell ID. NMR studies of modular protein structures and their interactions. Chem Rev 2004;104:3557–3566.
3. Zhang Y, Zuiderweg ER. The 70-kDa heat shock protein chaperone nucleotide-binding domain in solution unveiled as a molecular machine that can reorient its functional subdomains. Proc Natl Acad Sci USA 2004;101:10272–10277.
4. Fushman D, Xu R, Cowburn D. Direct determination of changes of interdomain orientation on ligation: use of the orientational dependence of ^{15}N NMR relaxation in Abl SH(32). Biochemistry 1999;38:10225–10230.
5. Fischer MWF, Losonczi JA, Weaver LJ, Prestegard JH. Domain orientation and dynamics in multidomain proteins from residual dipolar couplings. Biochemistry 1999;38:9013–9022.
6. Skrynnikov N, Goto N, Yang D, Choy W, Tolman J, Mueller G, Kay L. Orienting domains in proteins using dipolar couplings measured by liquid-state NMR: Differences in solution and crystal forms of maltodextrin binding protein loaded with beta-cyclodextrin. J Mol Biol 2000;295:1265–1273.
7. Goto NK, Skrynnikov NR, Dahlquist FW, Kay LE. What is the average conformation of bacteriophage T4 lysozyme in solution? A domain orientation study. J Mol Biol 2001;308:745–764.
8. Fushman D, Varadan R, Assfalg M, Walker O. Determining domain orientation in macromolecules by using spin-relaxation and residual dipolar coupling measurements. Progress NMR Spectroscopy 2004;44:189–214.
9. Chau V, Tobias JW, Bachmair A, Marriott D, Ecker DJ, Gonda DK, Varshavsky A. A multiubiquitin chain is confined to specific lysine in a targeted short-lived protein. Science 1989;243:1576–1583.
10. Finley D, Sadis S, Monia BP, Boucher P, Ecker DJ, Crooke ST, Chau V. Inhibition of proteolysis and cell cycle progression in a multiubiquitination-deficient yeast mutant. Mol Cell Biol 1994;14:5501–5509.
11. Varadan R, Walker O, Pickart C, Fushman D. Structural properties of polyubiquitin chains in solution. J Mol Biol 2002;324:637–647.
12. Cook WJ, Jeffrey LC, Carson M, Zhijian C, Pickart CM. Structure of a diubiquitin conjugate and a model for interaction with ubiquitin conjugating enzyme (E2). J Biol Chem 1992;267:16467–16471.
13. van Dijk ADJ, Fushman D, Bonvin AM. Various strategies of using residual dipolar couplings in NMR-driven protein docking: application to Lys48-linked di-ubiquitin and validation against ^{15}N-relaxation data. Proteins 2005;60:367–381.
14. Verma R, Peters NR, D'Onofrio M, Tochtrop GP, Sakamoto KM, Varadan R, Zhang MS, Coffino P, Fushman D, Deshaies RJ, King RW. Ubistatins inhibit proteasome-dependent degradation by binding the ubiquitin chain. Science 2004;306:117–120.
15. Varadan R, Assfalg M, Raasi S, Pickart C, Fushman D. Structural determinants for selective recognition of a Lys48-linked polyubiquitin chain by a UBA domain. Mol Cell 2005;18:687–698.
16. Woessner D. Nuclear spin relaxation in ellipsoids undergoing rotational brownian motion. J Chem Phys 1962;37:647–654.
17. Lipari G, Szabo A. Model-free approach to the interpretation of nuclear magnetic resonance relaxation in macromolecules. 1. Theory and range of validity. J Am Chem Soc 1982;104:4546–4559.
18. Baber JL, Szabo A, Tjandra N. Analysis of Slow Interdomain Motion of Macromolecules Using NMR Relaxation Data. J Am Chem Soc 2001;123:3953–3959.
19. Chang SL, Tjandra N. Analysis of NMR relaxation data of biomolecules with slow domain motions using wobble-in-a-cone approximation. J Am Chem Soc 2001;123:11484–11485.
20. Chang SL, Szabo A, Tjandra N. Temperature dependence of domain motions of calmodulin probed by NMR relaxation at multiple fields. J Am Chem Soc 2003;125:11379–11384.
21. La Penna G, Mormino M, Pioli F, Perico A, Fioravanti R, Gruschus JM, Ferretti JA. Smoluchowski dynamics of the vnd/NK-2 homeodomain from *Drosophila melanogaster*: first-order mode-coupling approximation. Biopolymers 1999;49:235–254.
22. La Penna G, Fausti S, Perico A, Ferretti JA. Smoluchowski dynamics of the vnd/NK-2 homeodomain from *Drosophila melanogaster*: second-order maximum correlation approximation. Biopolymers 2000;54:89–103.
23. Tugarinov V, Liang Z, Shapiro Y, Freed JH, Meirovitch E. A structural mode-coupling approach to ^{15}N NMR relaxation in proteins. J Am Chem Soc 2001;123:3055–3063.
24. Tugarinov V, Shapiro YE, Liang Z, Freed JH, Meirovitch E. A novel view of domain flexibility in E. coli adenylate kinase based on structural mode-coupling (15)N NMR relaxation. J Mol Biol 2002;315:155–170.
25. Shapiro YE, Kahana E, Tugarinov V, Liang Z, Freed JH, Meirovitch E. Domain flexibility in ligand-free and inhibitor-bound Escherichia coli adenylate kinase based on a mode-coupling analysis of 15N spin relaxation. Biochemistry 2002;41:6271–6281.
26. Varadan R, Assfalg M, Fushman D. Using NMR spectroscopy to monitor ubiquitin chain conformation and interactions with ubiquitin-binding domains. In: Deshaies RJ, editor. Ubiquitin and protein degradation. Methods in Enzymology, Vol. 399, part B; 2005. p 177–192.
27. Abragam A. The principles of nuclear magnetism. Oxford: Clarendon Press; 1961.
28. Press WH, Teukolsky SA, Vetterling WT, Flannery BP. Numerical recipes in C. New York: Cambridge University Press; 1992.
29. Jain NU, Venot A, Umemoto K, Leffler H, Prestegard JH. Distance mapping of protein-binding sites using spin-labeled oligosaccharide ligands. Protein Sci 2001;10:2393–2400.
30. Kosen PA. Spin labeling of proteins. Methods Enzymol 1989;177:86–121.
31. Fujiwara K, Tenno T, Sugasawa K, Jee JG, Ohki I, Kojima C, Tochio H, Hiroaki H, Hanaoka F, Shirakawa M. Structure of the ubiquitin-interacting motif of S5a bound to the ubiquitin-like domain of HR23B. J Biol Chem 2004;279:4760–4767.
32. de Alba E, Baber JL, Tjandra N. The use of residual dipolar coupling in concert with backbone relaxation rates to identify conformational exchange by NMR. J Am Chem Soc 1999;121:4282–4283.
33. Zweckstetter M, Bax A. Prediction of sterically induced alignment in a dilute liquid crystalline phase: aid to protein structure determination by NMR. J Am Chem Soc 2000;122:3791–3792.
34. Garcia de la Torre J, Huertas ML, Carrasco B. HYDRONMR: prediction of NMR relaxation of globular proteins from atomic-level structures and hydrodynamic calculations. J Magn Reson 2000;B147:138–146.
35. Cornilescu G, Marquardt JL, Ottiger M, Bax A. Validation of protein structure from anisotropic carbonyl chemical shifts in a dilute liquid crystalline phase. J Am Chem Soc 1998;120:6836–6837.
36. Koradi R, Billeter M, Wuthrich K. A program for display and analysis of macromolecular structures. J Mol Graph 1996;14:51–55.